Ultrathin single-crystal ZnO nanobelts: Ag-catalyzed growth and field emission property

2010 Nanotechnology 21 255701

Nanotechnology **21** (2010) 255701 (8pp) doi:10.1088/0957-4484/21/25/255701

Ultrathin single-crystal ZnO nanobelts: Ag-catalyzed growth and field emission property

G Z Xing[1,4], X S Fang[2], Z Zhang[1], D D Wang[1], X Huang[3], J Guo[3], L Liao[1], Z Zheng[1], H R Xu[1], T Yu[1], Z X Shen[1], C H A Huan[1], T C Sum[1], H Zhang[3] and T Wu[1,4]

[1] Division of Physics and Applied Physics, School of Physical and Mathematical Sciences, Nanyang Technological University, 637371, Singapore
[2] Department of Materials Science, Fudan University, Shanghai 200433, People's Republic of China
[3] School of Materials Science and Engineering, Nanyang Technological University, 639798, Singapore

E-mail: xing0012@ntu.edu.sg and tomwu@ntu.edu.sg

Received 18 December 2009, in final form 25 December 2009
Published 28 May 2010
Online at stacks.iop.org/Nano/21/255701

Abstract
We report the growth of ultrathin single-crystal ZnO nanobelts by using a Ag-catalyzed vapor transport method. Extensive transmission electron microscopy and atomic force microscopy measurements reveal that the thickness of the ultrathin ZnO nanobelts is ∼2 nm. Scanning electron microscopy and post-growth annealing studies suggest a '1D branching and 2D filling' growth process. Our results demonstrate the critical role of catalyst in the deterministic synthesis of nanomaterials with the desired morphology. In addition, these ultrafine nanobelts exhibit stable field emission with unprecedented high emission current density of 40.17 mA cm^{-2}. These bottom-up building blocks of ultrathin ZnO nanobelts may facilitate the construction of advanced electronic and photonic nanodevices.

(Some figures in this article are in colour only in the electronic version)

1. Introduction

One main theme in nanosciences and nanotechnologies is to develop facile methods to synthesize ultrathin nanostructures, aiming at enhancing the surface-to-volume ratio, exploring the novel electrical properties, and enabling high-density device integration. Recently, synthesis of ultrathin materials, including Ag, Au, ZnS, PbS, Si, CdSe, and Fe_3O_4, has been intensively pursued, and the significant breakthroughs have recently been reviewed [1]. In the area of nanomaterials research, one-dimensional (1D) nanoscale semiconductors have attracted lots of interest due to their promising applications in electronics, photonics, sensors, transducers, energy generation, and so on [2–6]. ZnO is one of the most intensively pursued nanomaterials. Yang *et al* have demonstrated the use of aligned nanowires in constructing UV lasers and solar cells [7, 8]. Following the discovery of ZnO nanobelts [9], Wang *et al* have pioneered the research fields of nanopiezotronics and energy scavenging devices using ZnO 1D nanomaterials [10–13]. Besides the wide band gap of 3.37 eV, ZnO has a large exciton binding energy (60 meV) at room temperature, thus it is able to provide stable band edge ultraviolet emission via the efficient exciton recombination process [14–16]. In a recent work, Yang's group reported on ultrathin nanorods of oxides including ZnO synthesized from acetate precursors using oleylamine and oleic acid as the capping and the structure directing agents, respectively [17]. However, although ZnO nanobelts [9, 18–20] and nanosheets [21, 22] are among the most studied nanomaterials, there has been no report on the reliable synthesis of single-crystal ZnO nanobelts.

In this paper, for the first time, we report the Ag-catalyzed growth of 2 nm ultrathin single-crystal ZnO nanobelts using a vapor transport method. Furthermore,

[4] Authors to whom any correspondence should be addressed.

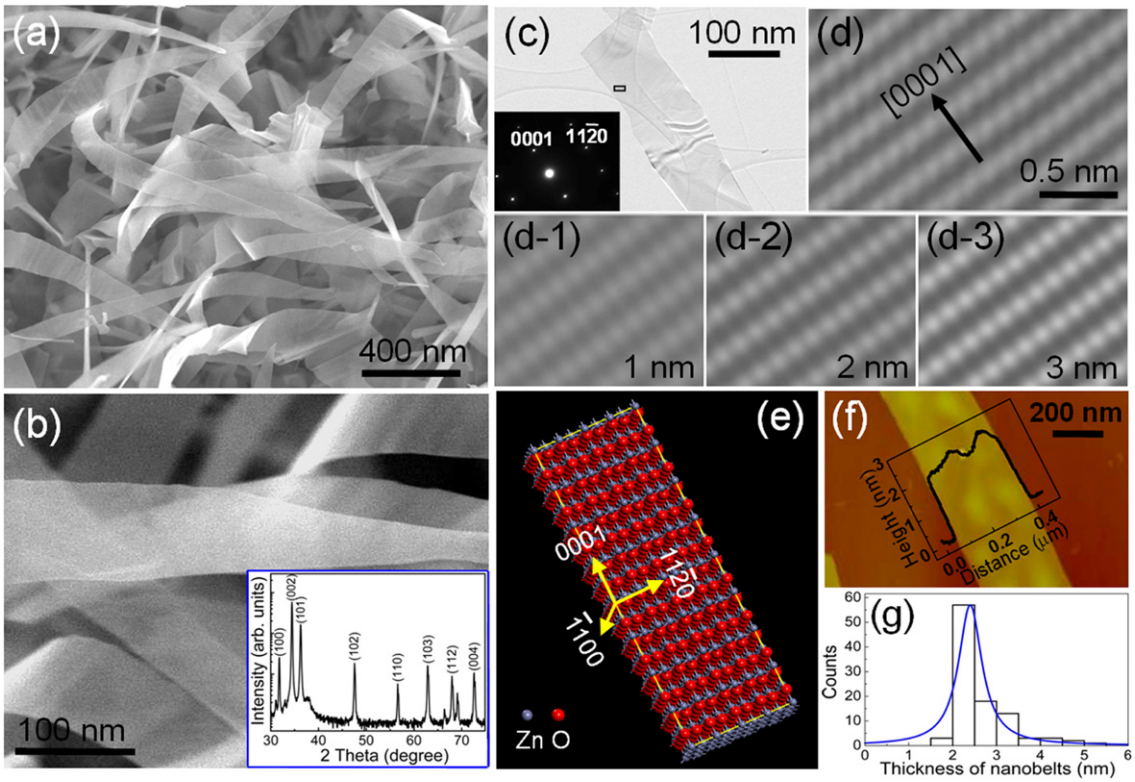

Figure 1. Representative (a) low- and (b) high-magnification FESEM images of the ultrathin ZnO nanobelts. The inset of (b) shows the XRD pattern of the ultrathin ZnO nanobelts. (c) TEM image and the corresponding SAED pattern. (d), (d-1), (d-2) and (d-3) Determination of the nanobelt thickness by comparing the HRTEM image with the simulation data. (e) Space-filling structure of a ZnO nanobelt composed of 8 ML stacked along the [$\bar{1}$100] direction. The small blue and large red balls represent Zn and O atoms, respectively. (f) AFM image of an ultrathin ZnO nanobelt and the corresponding height profile. (g) Histogram of thickness distribution for the ultrathin ZnO nanobelts.

in these free standing ultrathin nanobelts, stable field emission with unprecedented high emission current density of 40.17 mA cm^{-2} was observed due to the ultrathin nature of the ZnO nanobelts. Our results indicate that catalysts play critical roles in the deterministic morphology-controlled synthesis of nanomaterials. Equipped with unique ultrathin morphology, these ultrathin ZnO nanobelts may serve as bottom-up building blocks to facilitate the construction of advanced electronic and photonic nanodevices.

2. Experimental details

To synthesize ultrathin ZnO nanobelts, Zn powder (99.999%, Aldrich) was used as the vapor source and 2 nm Ag thin films as the catalyst. The vapor transport growth took place in a horizontal furnace, and the experimental setup has been described in previous reports [23–26]. Silicon substrates with a typical dimension of 6 mm × 8 mm were used. The temperatures of the source and the substrates were calibrated to be ∼500 and ∼475 °C, respectively. The relatively low growth temperature brings forth advantages such as low thermal budget, weak impurity diffusion, and reduced oxygen deficiency in the final products. Argon mixed with 5% oxygen was used as the carrying gas and the pressure inside the quartz furnace tube was kept at 20 mbar during the growth. After growing for a few minutes, a layer of white product was found on the substrates.

Field emission scanning electron microscopy (FESEM) images were acquired on a JOEL JSM-6700F, operated at 10 kV. The crystal structure of the samples was studied using x-ray diffraction (XRD) on a Bruker D8 advanced x-ray diffractometer with a Cu Kα source (λ = 0.154 18 nm). Structural characteristics and the local thickness of ZnO nanobelts were investigated with high-resolution transmission electron microscopy (HRTEM, JEOL 2100F) at an accelerating voltage of 200 kV. To determine the nanobelt thickness, simulation was performed using JEMS software (3.3111U2008), and the results were compared with the HRTEM images. The space-filling schematic of wurtzite ZnO nanobelts was illustrated using Materials Studio software (MS Modeling 4.1). Atomic force microscopy (AFM) images and height profiles were taken on a scanning probe microscope (Veeco Digital Instruments) with Si probe tips. Field emission properties were studied by using a diode structure with indium tin oxide (ITO) coated quartz as the anode and copper foil as the cathode. The inter-electrode, i.e. cathode-to-anode, distance was maintained at 100 μm and the experiments were conducted under a vacuum of ∼1.6 × 10^{-6} Pa.

3. Results and discussion

3.1. Characterization of ultrathin ZnO nanobelts

Figures 1(a) and (b) show the representative field emission scanning electron microscopy (FESEM) images of the

nanobelts grown on Si substrates. The nanobelts appear very uniform and transparent. They are several micrometers long and several hundred nanometers wide. These nanobelts taper off near the ends. The x-ray diffraction (XRD) pattern (inset of figure 1(b)) suggests a single-crystal wurtzite ZnO structure with lattice constants in agreement with the reported bulk data (JCPDS card No 36-1451, $P6_3mc$, $a = 3.25$ Å, $c = 5.21$ Å). As shown in the low-resolution transmission electron microscopy (TEM) image in figure 1(c), the nanobelt appears quite thin and homogeneous. The ripples on the transparent nanobelt may be due to the stress from the supporting carbon lacey film, which also reflects the ultrathin nature of the nanobelt. The selected area electron diffraction (SAED) pattern in the inset of figure 1(c) indicates a wurtzite structure, which is consistent with the XRD result. The growth direction was determined to be [0001] with $\pm(1\bar{1}00)$ top/bottom and $\pm(11\bar{2}0)$ side.

Previously, Wang *et al* have demonstrated that the thickness of ZnO nanobelts can be estimated by comparing the experimental high-resolution transmission electron microscopy (HRTEM) images with the simulation data [27]. In our TEM observations, defocusing was found to change the contrast of the inclined nanobelts. The best contrast of the nanobelts with an inclining angle of 50° was achieved at the defocus condition of −71 nm. The comparison of the HRTEM image in figure 1(d) with the simulation results in figures 1(d-1)–(d-3) using the same set of parameters indicates a nanobelt thickness of ∼2 nm, which corresponds to seven or eight ZnO monolayers. Figure 1(e) illustrates the space-filling structure of a ZnO nanobelt composed of 8 ML stacked along the $[\bar{1}100]$ direction, rendering a total thickness of ∼2.25 nm, which is close to the result shown in figure 1(d).

The nanobelt thickness was further determined by atomic force microscopy (AFM) after being transferred onto carefully cleaned Si substrates. Normally, to prepare samples for AFM scanning, nanomaterials need to be dispersed in organic solvents via ultrasonic shaking before being transferred onto solid substrates. However, the ultrathin nanobelts are very brittle and often damaged during the dispersion process. Therefore, we attached the nanobelts to the cleaned silicon substrates by using a simple physical transfer method, taking advantage of the static electrical force between the ultrathin nanobelts and the substrates when they are in proximity. AFM images were taken in contact mode to minimize the differences in interactions of the AFM tip with the ZnO nanobelts and the Si substrates. A representative AFM height image is shown in figure 1(f). The height profile across the nanobelt indicates a thickness of ∼2 nm, which is consistent with the TEM results. The nanobelt is quite uniform, and the same height was obtained at several positions on the nanobelt. The observed unevenness could be the result of residual particles on the substrate surface or inhomogeneous distribution of strain within the nanobelt due to the sample–substrate interaction. AFM data were taken on more than 100 nanobelts and consistent results were obtained. The surface morphology of the nanobelts appeared to be stable, and the nanobelt thickness remained the same during a period of two months. From the histogram in figure 1(g), the average thickness of the nanobelts was determined to be 2.4 ± 0.7 nm, thus the width-to-thickness ratio in the nanobelts is larger than 100. To the best of our knowledge, the nanobelts synthesized here are the thinnest among all the oxide nanobelts and nanosheets reported to date.

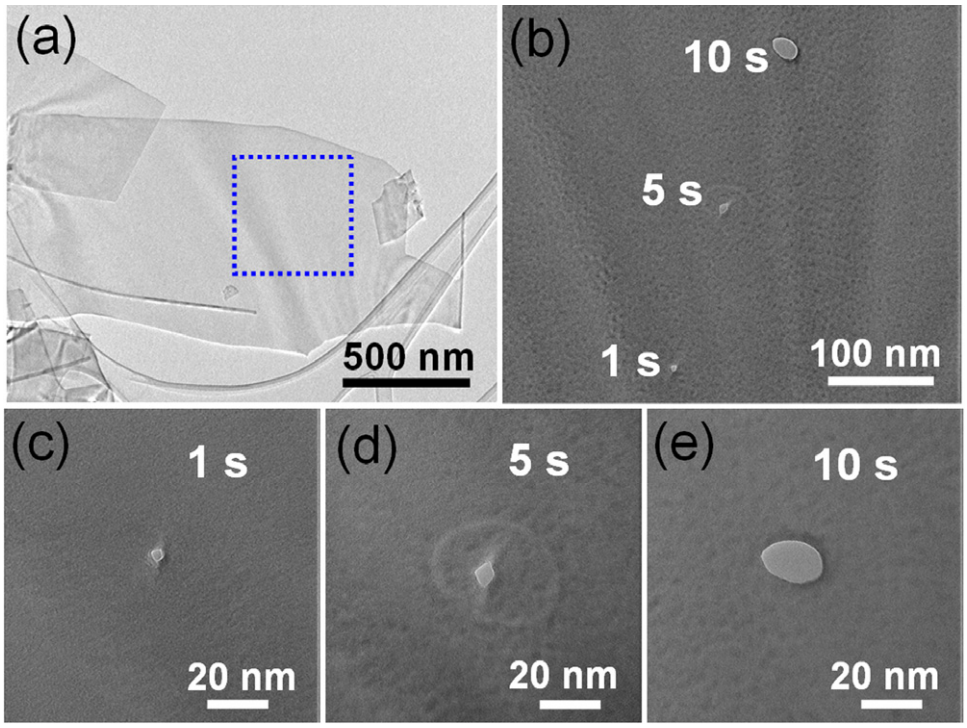

Figure 2. TEM images of (a) an ultrathin ZnO nanobelt and (b) three perforated holes created after irradiation with a focused electron beam in the area enclosed by the dashed lines in (a). Separate TEM images showing holes after irradiation of (c) 1 s, (d) 5 s, and (e) 10 s.

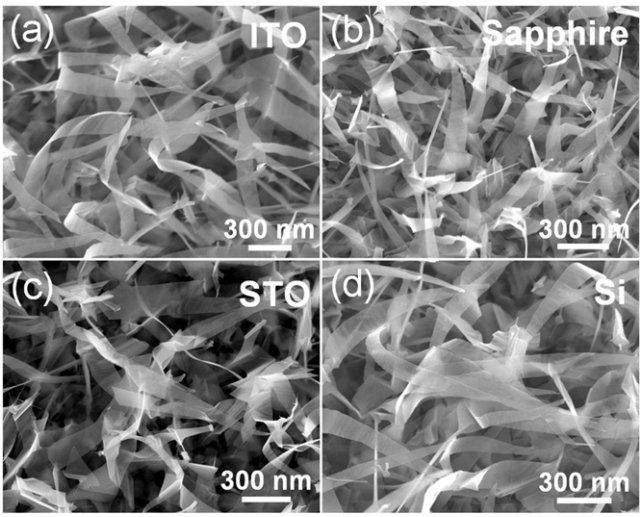

Figure 3. FESEM images of Ag-catalyzed ultrathin ZnO nanobelts grown on four different substrates, including indium tin oxide (ITO) coated quartz, Al_2O_3 (sapphire), $SrTiO_3$ (STO), and silicon (Si). There is no obvious substrate dependence.

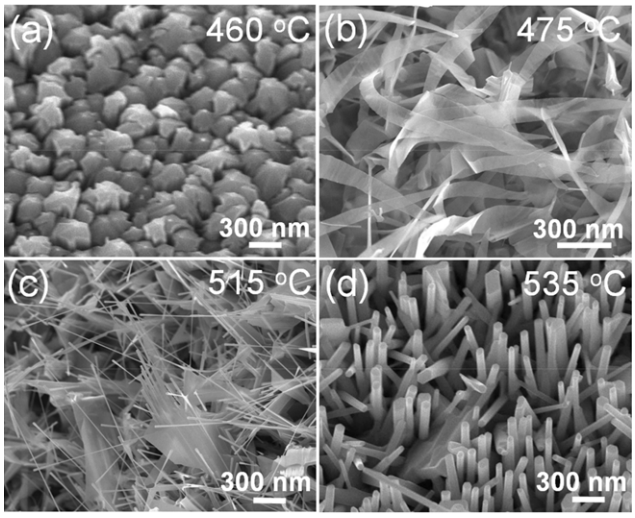

Figure 4. The temperature effects on the growth of ZnO nanostructures. Some typical growth results are highlighted: (a) polycrystals grown at 460 °C; (b) ultrathin nanobelts at 475 °C; (c) thicker nanobelts attached to nanowires at 515 °C; (d) nanorods at 535 °C.

The 2D morphology and the ultrathin nature of the ZnO nanobelts facilitate the *in situ* nanoscale machining inside TEM. Using a nanometer-sized focused electron beam at 200 kV, small holes were drilled onto the ultrathin ZnO nanobelts (figure 2). The experimental procedure is similar to a previous report [28]. Nanosized holes were generated on the nanobelts by controlling the irradiation duration of the focused electron beam. After electron beam irradiation for a few seconds, diamond-shaped nanoholes were observed. When the irradiation time increased to 10 s, the holes became larger and more rounded. Amorphous 'carbonized' regions were formed around the holes, and in these areas HRTEM imaging became difficult to obtain [29]. Due to the ultrafine thickness and the robust synthesis, ZnO nanobelts may serve as a good platform to advance nanoscale fabrication techniques on free standing materials.

One salient feature of our synthesis is that the substrate temperature is only 475 °C, lower than most vapor-based synthesis. This low growth temperature is amenable to a wide range of substrate materials, thus the ultrathin ZnO nanobelts can also be grown on substrates such as sapphire, ITO-coated quartz, and $SrTiO_3$. As shown in figure 3, we observed ultrathin ZnO nanobelts on all these substrates, and there appears to be no substrate dependence. It is important to note that the growth of the ultrathin ZnO nanobelts takes place within a fairly narrow temperature window from 470 to 505 °C. If the substrate temperature was lower than 470 °C, instead of 1D ZnO nanostructures, only polycrystalline grains were observed on the substrates (figure 4(a)). On the other hand, if the substrate temperature was higher than 505 °C, thicker nanobelts frequently appeared along with other nanostructures. The growth of nanowires or nanorods is notably favored at the high temperatures, which may be due to the thermally accelerated oxidation of Ag (figure 4(d)) [23]. In this case, the oxidized Ag no longer plays the role of catalyst, and the vapor–solid mechanism instead of the vapor–liquid–solid mechanism dictates the ZnO nanowire growth.

3.2. Ag-catalyzed growth mechanism

It is intriguing how Ag plays such a critical role of triggering the growth of ultrathin ZnO nanobelts, although it is well known that catalysts play deterministic roles in the synthesis of nanomaterials. Interestingly, Xia's group recently reported that Ag nanoparticles also promote the formation of ultrathin Au nanowires [30]. In previous efforts on the synthesis of ZnO nanowires and nanobelts, besides the most popular catalyst, Au, other metals such as Sn, Cu, and Ni were also explored [9, 31–35]. Recently, 15 metal catalysts of periods of IV, V, and VI were used to grow tin oxide nanowires, and their performances were compared [36]. On the theoretical aspect, recent first-principle calculations showed that the choice of transition metal catalyst determines the binding and diffusion of atomic precursors, which may lead to ultrathin morphologies [37, 38]. In the vapor transport growth of ZnO nanostructures, we found that the choices of catalyst dictate the morphology of the final products. As shown in figure 5, using several metal catalysts including Au, Pt, Cu, Sn, and Zn, we carried out growth experiments under identical conditions, and we found that only Ag can trigger the growth of ultrathin ZnO nanobelts.

In our experiments, the supersaturation of Zn vapor and the dynamic wetting and diffusion of Ag create a complex environment and may induce highly nonequilibrium growth [36, 39]. Considering their unique morphology, we hypothesize that these ultrathin ZnO nanobelts are formed in a continuous '1D branching and subsequent 2D interspace filling' process [40]. This growth process simultaneously involves substantial precursor migration and effective mass

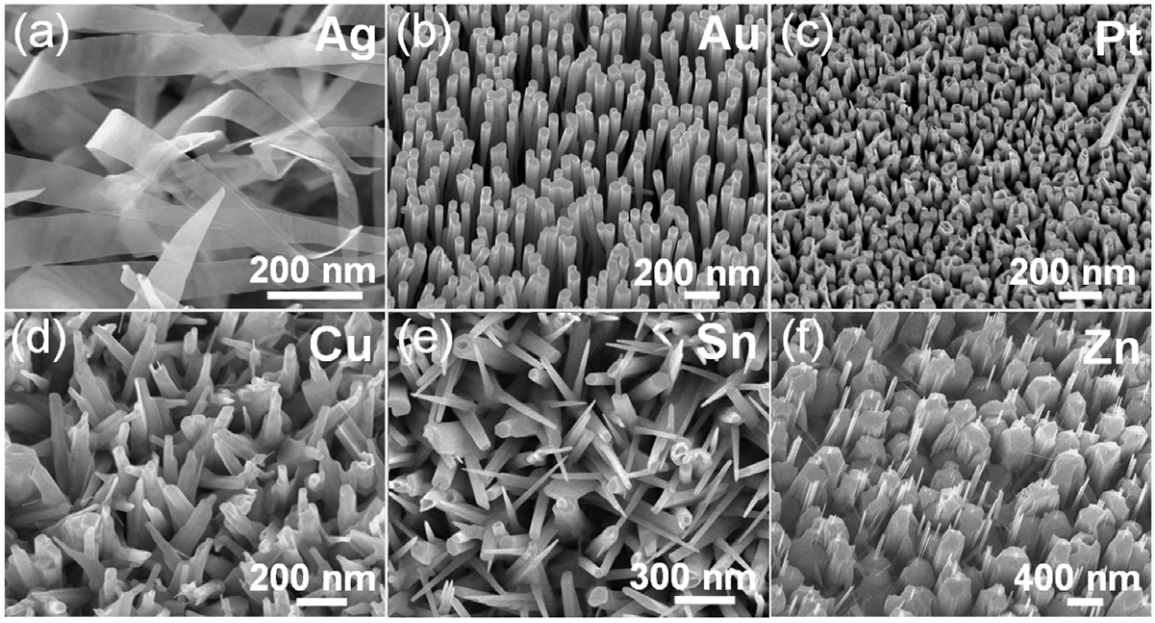

Figure 5. FESEM images of ZnO nanostructures grown with different metal catalysts under identical experimental conditions. Only Ag induces the growth of ultrathin nanobelts; other metal catalysts including Au, Pt, Cu, Sn and Zn lead to the formation of either nanowires or nanorods.

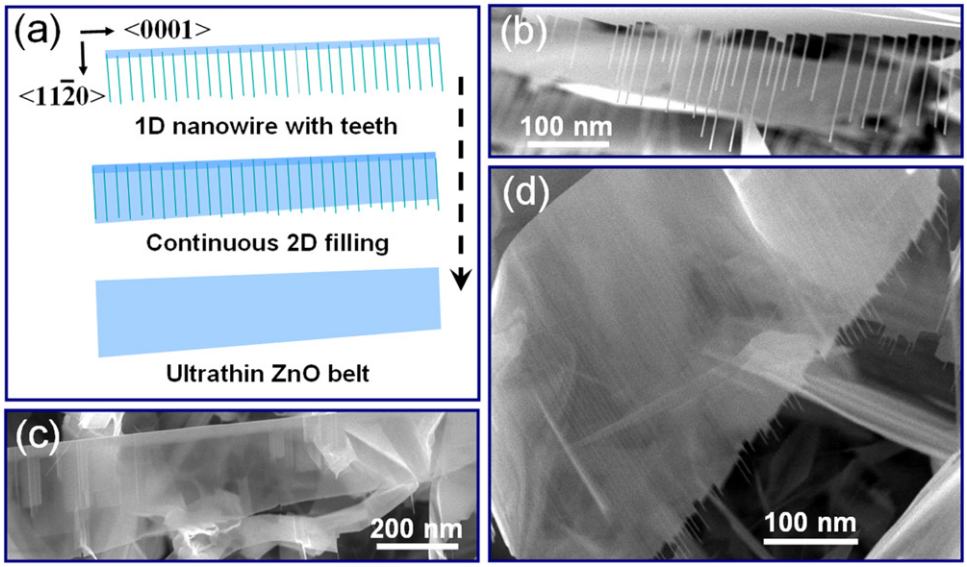

Figure 6. (a) Schematic illustration of the '1D branching and 2D filling' growth process. (b)–(d) Representative FESEM images of ultrathin ZnO nanostructures at various growth stages.

redistribution. During the growth, Ag in its melting state may serve as a soft template to assist the vapor condensation and the subsequent nanobelt growth. Figure 6 shows a schematic of the growth process along with several FESEM images of ultrathin ZnO nanobelts at various growth stages. For group II–VI semiconductors with a wurtzite crystal structure, the characteristic polar surfaces, i.e. cation- or anion-terminated atomic planes, can induce asymmetric growth, leading to the formation of unique nanostructures, such as nanocombs, nanosaws, and nanocantilevers [41, 42]. As illustrated in figure 6(a), ZnO nanowires may grow first along the [0001] direction, then ultrafine nanoteeth grow epitaxially along the $\langle 11\bar{2}0 \rangle$ direction from the parent nanowires. Such nanocomb-like structures were frequently observed, and one example is shown in figure 6(b). Finally, the ultrathin nanobelts are formed with vapor condensation selectively on the concave corner sites between the branches, where the chemical potential is lower than the convex and the flat surface sites. Figure 6(c) shows a particular example of a ZnO nanobelt with a thicker nanowire residing on the top edge. Since the

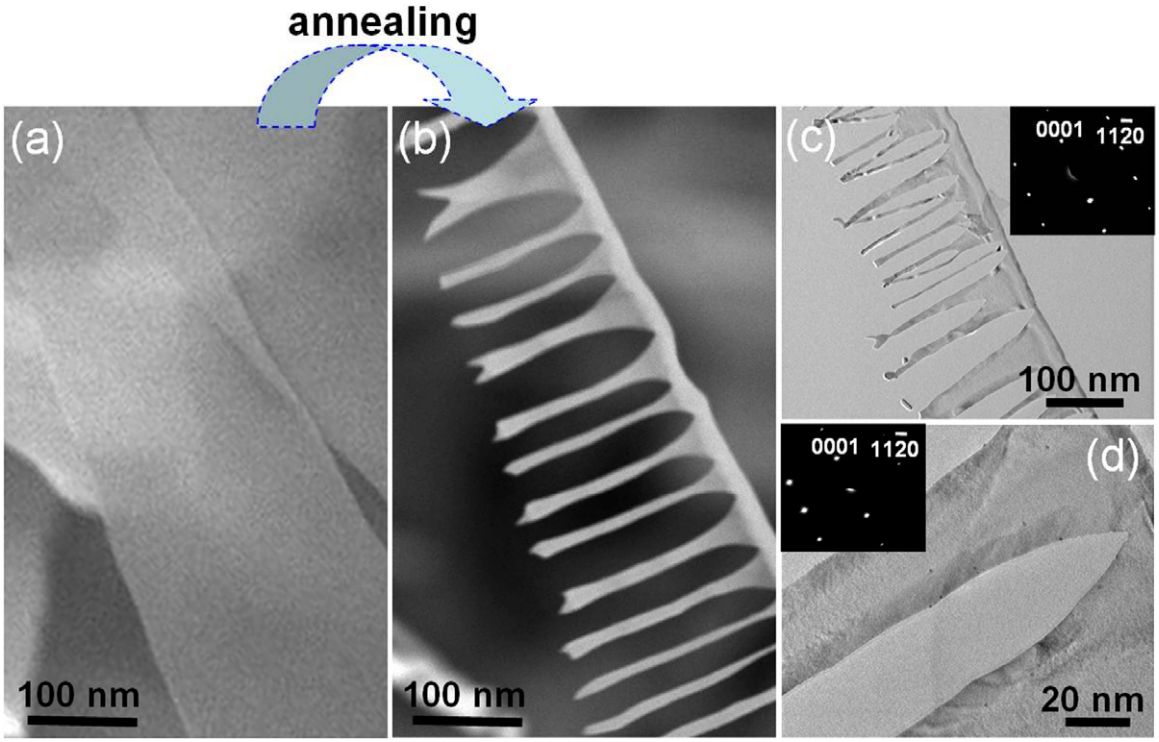

Figure 7. FESEM images of (a) as-grown ultrathin ZnO nanobelts and (b) comb-like nanostructures obtained by annealing the as-grown ultrathin nanobelts at 500 °C in air for 1 h. (c), (d) TEM images of nanocombs and the corresponding SEAD patterns (insets).

growth took place in an oxygen-deficient environment, Zn supersaturation may first lead to the formation of zinc suboxide (ZnO_x, $x < 1$). Considering that the furnace temperature is much higher than the melting point of ZnO_x [43], substantial material migration and effective mass redistribution may occur before the eventual complete oxidization and crystallization. Since Ag has the highest thermal conductivity among all metals [44], the absorbed surface atoms or molecules are equipped with high mobility and are distributed uniformly, occupying the energetically favorable sites. Interestingly, nanobelts with teeth on one side were frequently observed (figure 6(d)), which provides strong support to our proposed growth model.

Post-growth annealing experiments further corroborate the proposed growth model. The as-grown ultrathin ZnO nanobelts were annealed at 500 °C in air for 1 h. As shown in the FESEM image in figures 7(a) and (b), interestingly, the smooth nanobelts transform into nanocombs after annealing, which indicates substantial mass redistribution at the annealing temperature. In the TEM images in figures 7(c) and (d), the thicker edges of the comb teeth can be attributed to the thermally activated diffusion and the mass redistribution. The corresponding SAED patterns in the insets confirm that the crystal structure does not change during the process of annealing and morphological transformation.

3.3. Field emission properties

Considering that decreased dimension often renders unique functionalities [1], we characterized the field emission properties of the ultrathin ZnO nanobelts. We also synthesized ZnO nanowires with an average diameter of 50 nm using Au as catalyst, and carried out a comparative study. The measurements took place at a pressure of $\sim 1.6 \times 10^{-6}$ Pa and the distance between the sample and the anode was kept at ~ 100 μm. As shown in figure 8(a), at a current density of 1 mA cm^{-2}, a threshold field of 8.5 V μm^{-1} was observed. Importantly, at a macroscopic field of 11 V μm^{-1}, an emission current density of ca. 40.17 mA cm^{-2} was achieved in the ultrathin nanobelts, which rivals the best values in the previous reports on nanomaterials including ZnO, ZnS, Si, AlN, CNTs, and so on [45]. In comparison, the nanowires exhibited unstable emission, and breakdown often occurred at electric field <10 V μm^{-1}. The comparative results indicate that the ultrathin ZnO nanobelts have good field emission properties, which may be attributed to their unique morphology and the associated electronic structures under nanoscale confinement.

The Fowler–Nordheim plot in the inset of figure 8(a) was fitted to the linear relationship given by

$$\ln(J/E^2) = \ln(A\beta^2/\varphi) - B\varphi^{3/2}/\beta E \qquad (1)$$

where $A = 1.54 \times 10^{-6}$ A eV V^{-2}, $B = 6.83 \times 10^3$ eV$^{-3/2}$ V μm^{-1}, β is the field-enhancement factor, and the work function $\varphi = 5.3$ eV for ZnO [45]. The calculated field-enhancement factor β of the ultrathin ZnO nanobelts is $\sim$700. In addition, as presented in figure 8(b), the emission current from the ultrathin nanobelts is quite stable, which is crucial for applications. An average emission current density of 7.4 mA cm^{-2} was obtained at a constant electric field

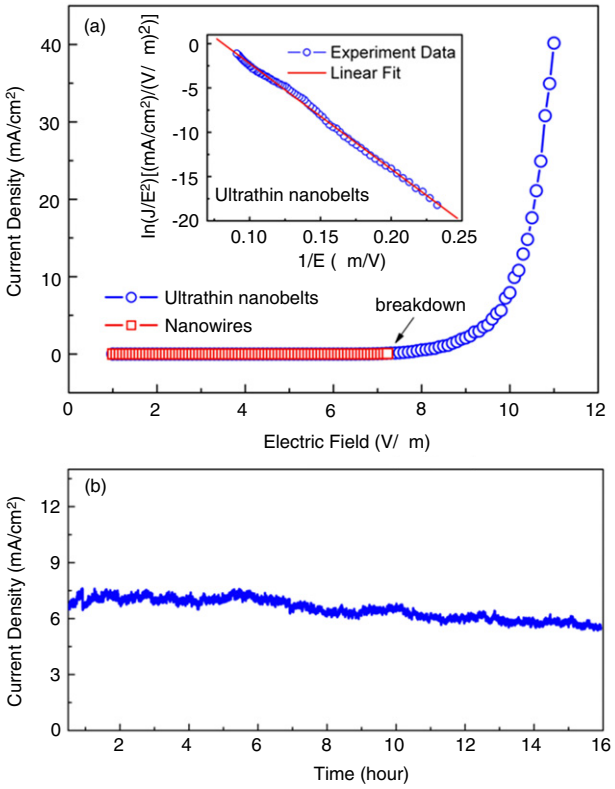

Figure 8. (a) Field emission current versus electric field curves of ultrathin ZnO nanobelts, in comparison with that obtained in ZnO nanowires. Inset is the corresponding Fowler–Nordheim plot for nanobelts. (b) Emission current density versus time data recorded on ultrathin ZnO nanobelts at an electric field of 10 V μm^{-1}.

of 10 V μm^{-1}. The emission stability was maintained for >16 h, and the fluctuation is ∼14%. In terms of emission current density and stability, the ultrathin ZnO nanobelts compare favorably with other ZnO nanostructures reported in the literature [45], and they may find applications in future display devices.

4. Conclusions

In summary, we report that 2 nm ultrathin ZnO nanobelts with high uniformity and crystalline quality can be reliably grown using a simple Ag-catalyzed vapor transport method and field emission properties were observed. This strong correlation between catalyst and morphology in the nanomaterials synthesis may manifest in other materials systems, and research along this line will help to advance our understanding on the nanomaterials growth. Compared with the thin film counterparts, the ultrathin nanobelts do not suffer from the growth-induced surface roughness, and the absence of film–substrate interaction in the free standing nanobelts may help to reveal novel physical properties. In the future, these ultrathin ZnO nanobelts may serve as bottom-up building blocks to facilitate the construction of advanced electronic and photonic devices, such as nanoscale resonant tunneling devices, field-effect transistors, and light-emitting devices.

Acknowledgments

This work was supported by the Singapore Ministry of Education Research Grants (SUG 20/06 and RG 46/07). G Z Xing acknowledges the support from Singapore Millennium Foundation Scholarship, Singapore.

References

[1] Cademartiri L and Ozin G A 2008 *Adv. Mater.* **20** 1
[2] Duan X, Huang Y, Agarwal R and Lieber C M 2003 *Nature* **421** 241
[3] Hu J, Odom T W and Lieber C M 1999 *Acc. Chem. Res.* **32** 435
[4] Xia Y N, Yang P D, Sun Y G, Wu Y Y, Mayers B, Gates B, Yin Y D, Kim F and Yan Y Q 2003 *Adv. Mater.* **15** 353
[5] Wang Z L 2004 *J. Phys.: Condens. Matter* **16** 829
[6] Lu J G, Chang P and Fan Z 2006 *Mater. Sci. Eng.* R **52** 49
[7] Huang M H, Mao S, Feick H, Yan H, Wu Y, Kind H, Weber E, Russo R and Yang P 2001 *Science* **292** 1897
[8] Law M, Greene L E, Johnson J C, Saykally R and Yang P 2005 *Nat. Mater.* **4** 455
[9] Pan Z W, Dai Z R and Wang Z L 2001 *Science* **291** 1947
[10] Wang Z L and Song J H 2006 *Science* **312** 242
[11] Wang X D, Song J H, Liu J and Wang Z L 2007 *Science* **316** 102
[12] Wang Z L 2007 *Adv. Mater.* **19** 889
[13] Qin Y, Wang X and Wang Z L 2008 *Nature* **451** 809
[14] Claus K, Robert H, Johannes F and Heinz K 2007 *Phys. Rev.* B **75** 115203
[15] Claus K 2007 *ChemPhysChem* **8** 782
[16] Gargas D J, Toimil-Molares M E and Yang P 2009 *J. Am. Chem. Soc.* **131** 2125
[17] Huo Z, Tsung C-K, Huang W, Fardy M, Yan R, Zhang X, Li Y and Yang P 2009 *Nano Lett.* **9** 1260
[18] Wang W Z, Zeng B Q, Yang J, Poudel B, Huang J Y, Naughton M J and Ren Z F 2006 *Adv. Mater.* **18** 3275
[19] Wang X D, Ding Y, Summers C J and Wang Z L 2004 *J. Phys. Chem.* B **108** 8773
[20] Li Y B, Bando Y, Sato T and Kurashima K 2002 *Appl. Phys. Lett.* **81** 144
[21] Hu J Q, Bando Y, Zhan J H, Li Y B and Sekiguchi T 2003 *Appl. Phys. Lett.* **83** 4414
[22] Chen S J, Liu Y C, Shao C L, Mu R, Lu Y M, Zhang J Y, Shen D Z and Fan X W 2005 *Adv. Mater.* **17** 586
[23] Zhang Z, Wang S J, Yu T and Wu T 2007 *J. Phys. Chem.* C **111** 17500
[24] Zhang Z, Sun Y, Zhao Y, Li G and Wu T 2008 *Appl. Phys. Lett.* **92** 103113
[25] Xing G Z *et al* 2008 *Adv. Mater.* **20** 3521
[26] Xing G Z, Yi J B, Wang D D, Liao L, Yu T, Shen Z X, Huan C H A, Sum T C, Ding J and Wu T 2009 *Phys. Rev.* B **79** 174406
[27] Ding Y and Wang Z L 2004 *J. Phys. Chem.* B **108** 12280
[28] Zhan J H, Bando Y, Hu J and Golberg D 2006 *Appl. Phys. Lett.* **89** 243111
[29] Cademartiri L, Malakooti R, O'Brien P G, Migliori A, Petrov S, Kherani N P and Ozin G A 2008 *Angew. Chem. Int. Edn* **47** 3814
[30] Lu X, Yavuz M S, Tuan H-Y, Korgel B A and Xia Y 2008 *J. Am. Chem. Soc.* **130** 8900
[31] Kong Y C, Yu D P, Zhang B, Fang W and Feng S Q 2001 *Appl. Phys. Lett.* **78** 407
[32] Gao P X, Ding Y and Wang Z L 2003 *Nano Lett.* **3** 1315
[33] Li S Y, Lee C Y and Tseng T Y 2003 *J. Cryst. Growth* **247** 357

[34] Rybczynski J, Banerjee D, Kosiorek A, Giersig M and Ren Z F 2004 *Nano Lett.* **4** 2037–40
[35] Xu C X and Sun X W 2003 *Appl. Phys. Lett.* **83** 3806
[36] Nguyen P, Ng H T and Meyyappan M 2005 *Adv. Mater.* **17** 1773
[37] Fan X, Buczko R, Puretzky A A, Geohegan D B, Howe J Y, Pantelides S T and Pennycook S J 2003 *Phys. Rev. Lett.* **90** 145501
[38] Yazyev O V and Katsnelson M I 2008 *Phys. Rev. Lett.* **100** 47209
[39] Ng H T, Li J, Smith M K, Nguyen P, Cassell A, Han J and Meyyappan M 2003 *Science* **300** 1249
[40] Park J H, Choi H J, Choi Y J, Sohn S H and Park J G 2004 *J. Mater. Chem.* **14** 35
[41] Wang Z L, Kong X Y and Zuo J M 2003 *Phys. Rev. Lett.* **91** 185502
[42] Kong X Y and Wang Z L 2003 *Nano Lett.* **3** 1625
[43] Yao B D, Chan Y F and Wang N 2002 *Appl. Phys. Lett.* **81** 757
[44] Mohanty P, Yoon I, Kang T, Seo K, Varadwaj K S K, Choi W, Park Q H, Ahn J P, Suh Y D and Ihee H 2007 *J. Am. Chem. Soc.* **129** 9576
[45] Fang X S, Bando Y, Gautam U K, Ye C H and Golberg D 2008 *J. Mater. Chem.* **18** 509